RSC Advances

PAPER

View Article Online
View Journal | View Issue

Cite this: *RSC Adv.*, 2015, **5**, 57437

Graphene and chiral nematic liquid crystals: a focus on lasing†

Ammar A. Khan,[a] Muhammad A. Bin-Kamarudin,[a] Piran. R. Kidambi,[b] Stephan Hofmann,[b] Timothy D. Wilkinson[a] and Malik M. Qasim*[a]

Received 19th May 2015
Accepted 22nd June 2015

DOI: 10.1039/c5ra09415a

www.rsc.org/advances

This work presents the interaction of self-assembled liquid crystalline (LC) unidimensional photonic structures on the surface of polycrystalline graphene. Further, this surface effect is studied through different substrate geometries in the test devices. Primarily, these devices are characterised through polarizing optical microscopy (POM) and their laser emission features in the dye-doped chiral systems. Then the conductive nature of graphene is utilized to apply external electric fields to the photonic medium and its effect is envisaged. These graphene-based devices demonstrate a unique result in polarizing optical micrographs and electro-optic responses which indicates the presence of multidirectional domain formations. Additionally, the LC band-edge lasing from graphene cells is found to be anisotropic and depends on the directionality of the optical pump. This work attempts to lay the foundation for the implementation of a new class of defused chiral nematic liquid crystal based devices *e.g.* optical filters, notch filters, colour reflectors, and light shutters and may add toward the knowledge base necessary in the substitution of Indium Tin Oxide (ITO) with graphene in traditional LC based display devices.

1. Introduction

There is considerable interest in the development of device applications using chiral nematic liquid crystals (LCs). These self-assembled, LC photonic band-gaps, demonstrate distinct, easily tuneable band edges,[1–3] which yield selective light reflections, allowing them to be used in device applications such as thermometers,[4] notch filters[5] and band-edge lasers,[6–8] to name a few applications. Band-edge organic lasers based upon chiral nematic LCs have stimulated significant research interest due to a remarkable combination of characteristics, such as ease of fabrication, single-mode emission, wide-band wavelength tunability, in micron-sized resonator structures where the thickness of the active film is less than the dimension of a human hair.[6,9,10] Interestingly, graphene is a single-atom thick material, possesses a honeycomb lattice and has shown promising properties *i.e.* optically transparent, high strength, high current density, high charge mobility and as thin flexible substrate.[4] In addition to these intrinsic properties of graphene, the interaction of graphene's surface with nematic liquid crystals (LC) has also been an area of interest in several studies.[11–14] It has been reported that a thin layer of LC molecules on the surface of graphene exhibits significant π–π stacking at the interface, which induces highly ordered packing with respect to each graphene domain.[15,16] Furthermore, the boundaries of these domains could be easily observed under a polarizing optical microscope by exploiting the birefringence of the nematic LC material.[12]

Here we explore the interaction of a unidimensional (1D) chiral nematic photonic structure on the surface of chemical vapour deposition (CVD) grown polycrystalline graphene in a sandwich cell geometry and study its effect on their laser emission. To envisage the effect of the graphene layer on the photonic structure, we have fabricated and characterised four sets of two substrate sandwich device architectures; graphene (Gr)–Gr, Gr–ITO (indium tin oxide), ITO–ITO (with and without polyimide (PI) alignment layers). An optimised chiral nematic lasing mixture was capillary filled into these devices (ESI; Fig. S1c and d†) to probe laser emission.[17]

2. Methods

Graphene growth was performed *via* CVD on polycrystalline Cu foils as reported.[18,19] The synthesised graphene was transferred from the Cu foil to a pre-cleaned glass substrate by using polystyrene which acts as a polymer support layer (PS, M_w 35k, 2% w/w in toluene) and an acid ($FeCl_3$ aq., 0.5 M) to etch the Cu. This was followed by a wash in a warm ethyl acetate bath to dissolve off the supporting polymer layer. The graphene layer

[a]*Centre of Molecular Materials for Photonics and Electronics, Department of Engineering, University of Cambridge, 9 J.J. Thomson Avenue, Cambridge, CB3 0FA, UK. E-mail: qmm20@cam.ac.uk*

[b]*Department of Engineering, University of Cambridge, Cambridge, CB3 0FA, UK*

† Electronic supplementary information (ESI) available. See DOI: 10.1039/c5ra09415a

was characterised by Raman microscopy and scanning electron microscopy (ESI; Fig. S1a and b†).

For this experimental study, four sets of sandwich cell devices were fabricated from two pieces of glass substrates with graphene (Gr) and/or ITO as conductive layers; Gr–Gr, Gr–ITO whereas, in the case of ITO–ITO two sets of cells were devised (with and without PI alignment layer on ITO surface). In the case of Gr-substrate, a metallic contact was made at the short-edge of pre-cleaned glass substrate by depositing a thin layer of Ni (~50 nm) strip, followed by a transfer of graphene layer across the substrate using the procedure mentioned above. On the other hand, commercial ITO coated glass (Instrument Glasses Inc. UK) was used as a second conductive substrate with and without alignment layers. The substrates were bonded together using glue that contained ~9 μm spacer glass beads.

The lasing mixture utilized as reported; consisted of a PM 597 1% w/w laser dye doped mixture of a commercial nematic LC BL006 (Merck).[17] A right-handed chiral dopant BDH-1281 was added to the mixture as 4.2% w/w concentration to obtain a 1D photonic band. The concentration of chiral dopant has been chosen carefully such that the long edge of the gap matches the dye fluorescence maximum. The mixture was heated to 130 °C for 10 minutes and then left overnight in an oven at 80 °C for a homogeneous thermal diffusion. Then this optimized mixture was capillary filled into fabricated cells at room temperature.

For the optical pump source, a pulsed (1 Hz, 3 ns) Q-switched, frequency doubled 532 nm Nd-YAG laser, (NewWave research Polaris II) was used (spot size ≈ 150 μm). The pump light was converted to right hand circular using a λ/4 plate, and the intensity was modulated using a half-wave plate/polarizer arrangement. The output light was coupled from a fibre into an ocean optics HR-2000+ spectrometer, with a 0.3 nm resolution, and the pump energy was measured using an energy meter (PD10 silicon photodiode head with Laserstar energy meter, Ophir).

3. Result and discussion

Polarizing optical micrographs (POM) of the chiral nematic mixture were recorded to visualize the effect of graphene surface in the different test cell configurations (LC textures of these devices are illustrated in Fig. 1). The ITO–ITO cell (with alignment layers) displays a standard Grandjean texture as reported,[17] whereas the ITO–ITO cell (without alignment layers) displays a texture indicative of a multi-domain surface superimposed on the Grandjean texture (oily streaks can be seen in Fig. 1d). On the other hand, Gr–Gr test cells exhibited a relatively more disordered texture (Fig. 1c) and similar texture was observed in the case of the hybrid device (Gr–ITO). These disordered textures over a graphene sheet display similarities to the presence of degenerated planar alignment.[20,21] The overall perceptible chiral nematic (N*LC) textures in the graphene cells appear to be very similar to those in the ITO–ITO cell without PI alignment layers, but interaction between graphene and the LC molecules has been discussed in previous studies[12] where these rod-like LC molecules tend to align with the honey-comb lattice of graphene-domains and can be expected to manifest itself in the output of N*LC medium.

Several studies have reported[11–14] about the alignment of nematic LCs on the surface of graphene, due to the chemical nature of LC material and graphene sheet. Strong π–π interaction has been observed which appear as nematic phase textures (domain boundaries) under the POM with multi-domain orientation corresponding to graphene sheet lattice. Chiral nematic LCs, on the other hand, has layered structure of nematic phase and form twisted helices when confined between two surfaces. There is a possibility that a few layers of chiral nematic LC, near to the graphene surface, exhibit strong π–π interaction and induce a multi-oriented nematic texture. However, this effect tends to fade away when further layers of chiral nematic LC assemble-up to from a twisted helix. Hence,

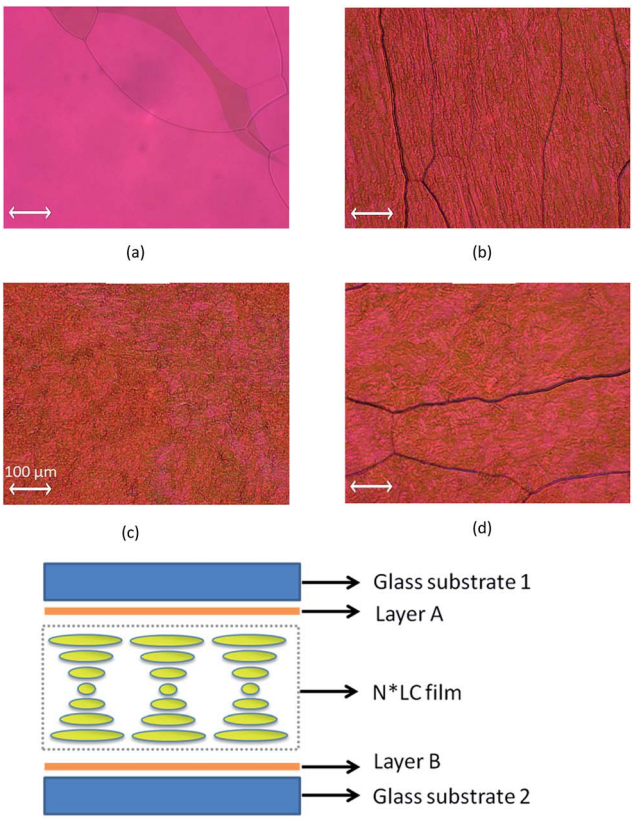

Cell Architecture	Layer A	Layer B
ITO - ITO	ITO with polyimide alignment layers	ITO with polyimide alignment layers
Gr - ITO	ITO without polyimide alignment layers	Graphene
Gr - Gr	Graphene	Graphene
ITO - ITO - NA	ITO without polyimide alignment layers	ITO without polyimide alignment layers

(e)

Fig. 1 Optical micrographs of the textures of (a) ITO–ITO with alignment layers, (b) ITO–ITO without alignment layers, (c) Gr–ITO without alignment, and (d) Gr–Gr (these micrographs were recorded as 20× magnification). (e) Illustration of the four different sandwich cell architectures primarily studied in this work.

no clear or significant texture difference has been seen in the hybrid (Gr–ITO) and conventional test cell (ITO–ITO) (Fig. 1).

A typical chiral nematic (N*LC) test cell with a 1D photonic band structure demonstrates a particular light reflection pattern under the white light illumination and shows strong dependency on the angle of incident light rays. However, test cells with Gr-electrode have shown unexpected wide angle distribution of the light reflection pattern under ambient room light when compared with an ITO–ITO cell (PI alignment layers). Further, it can be seen that the graphene sheet appears as a strip with distinct edges across the cell (Fig. 2). The noticeable change can been observed in the reflected colour, either at the edges or the area of cell where graphene surface is absent. It is postulated, that this is indicative of tilted, multi-directional 1D standing helices of this photonic structure within a device. Additionally, these tilted chiral domains on the graphene electrode may result in an increase in the angular spread of the reflection spectra. The photograph (Fig. 2b) exactly illustrates this, N*LC material above the graphene layer can be seen as visibly iridescent green/orange colours which are contributions from the photonic-reflection band (stop-band) even at non-specular angles. An illustration of this increased angular distribution can be seen in Fig. 2(f).

For the comparison a nematic LC (BL006) and a chiral LC mixture is spin-coated on a graphene sheet as a single substrate. In the case of BL006, a thin layer on the graphene surface, the material exhibits multi-domain orientations with a directional reliant birefringence as reported in other literature.[15] The LC texture displays a change in the colour of each domain upon the rotation from 0° to 90° (Fig. 3a and b), domains that have the similar colour (same birefringence) changed from darker to bright and *vice versa*. However, In the case of chiral nematic LC layer no effect has been observed in birefringence of the graphene substrate when rotated from 0° to 90°. This is an expected response from typical standing chiral nematic helices, even though; random domain features were present due the graphene surface.

There seems to be a unique domain structure in every test cell, in particular, the presence of disordered multi-domain structures in graphene test cells. These features became more prominent when an electric field was applied across these devices. Gr-electrode test cells displayed exceptional electro-optical transitions. Initially, it seemed as random Grandjean domain texture to a finger print transition then this is followed by the appearance of localized focal conic textures before the helices were completely unwound to yield an optically isotropic phase (dark state under crossed polarizer). This signifies that graphene surface is contributing to both planar and homeotropic alignments within the test cell,[22] see Fig. 6 and S2,† under the application of an applied E-field. To cross examine this behaviour, the applied electric field effect was studied in ITO–ITO cells with planar and homeotropic alignments filled with the same lasing mixture (ESI, Fig. S2 and S3† respectively). However, this unique textural transition was only observed in graphene electrode cells.

To collectively study the self-assembly of photonic structure and electro-optic response on the graphene electrode, these

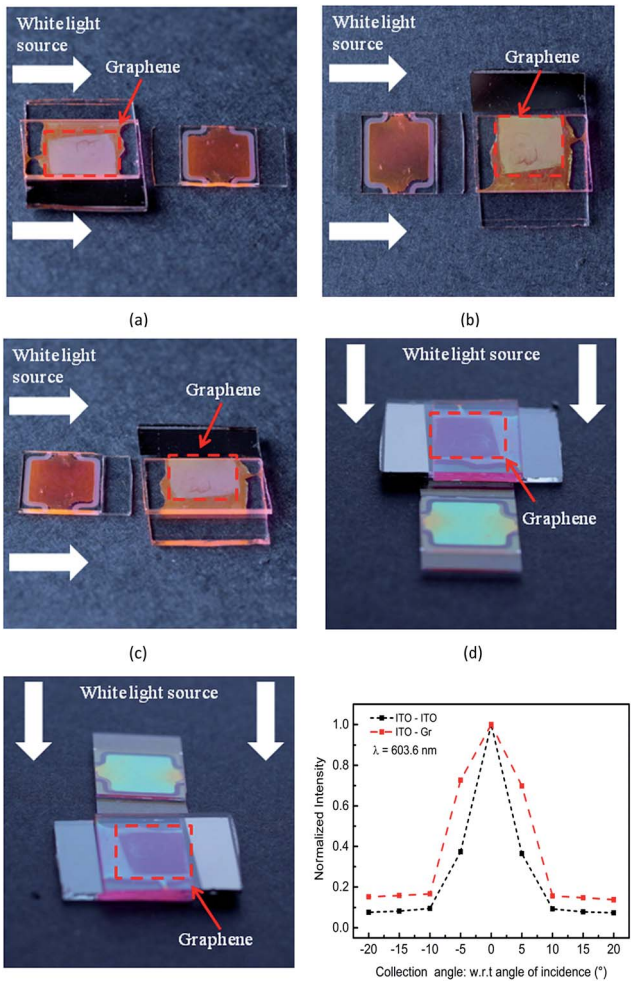

Fig. 2 Illustration the diffuse nature of reflections from the disordered photonic band gap, photographs of a Gr–ITO cell and an ITO–ITO (PI) cell are taken at different angles under diffused room lighting, (a) left-hand side of the cells, (b) on top of the cells, (c) right-hand side of the cells. Photos of the cells at specular reflection angles can be seen in (d) top side of the cells, and (e) bottom side of the cells. (f) Intensity of reflected white light as a function of collection angle (at an angle of incidence fixed at 30°).

four sets of test cells (Gr–Gr, Gr–ITO, ITO–ITO with and without planner alignments) were capillary filled with a dye-doped optimised chiral mixture (mixture details are mentioned above). Then lasing characteristics of each test cell were recorded as a spectral output of each device under pulsed 532 nm optical pump (illustrated in Fig. 4). ITO–ITO cell (with alignment layers) demonstrated a narrow peak at the band edge with a well-defined threshold, corresponding to resonant lasing[6] (Fig. 4a). The emission spectrum in the case of cells containing graphene sheets (Gr–Gr) (Fig. 4b) consists of many discrete peaks that overlay on the dye emission spectrum (ESI, Fig. S1b†). It is assumed that these discrete peaks correspond to micron-sized lasing for random domains, each with a different effective photonic band-edge. These micron sized domains are thought to be an effect of the interaction of the graphene alignment layers with the chiral nematic LC layer. The pump threshold for these modes is measured to be much higher that

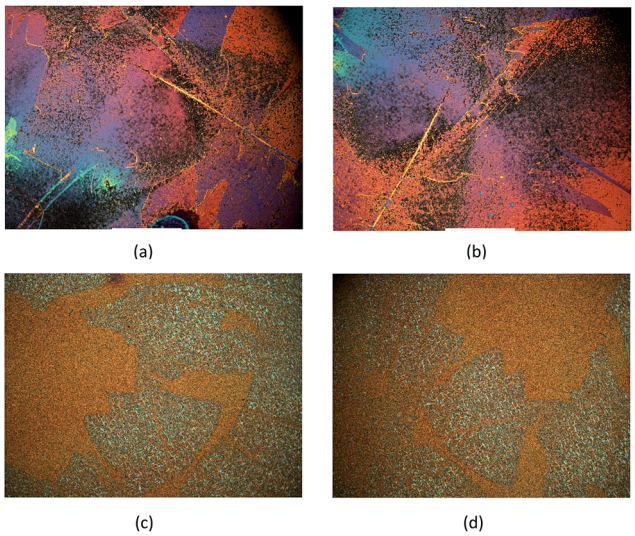

Fig. 3 Optical micrographs of the textures of BL006 with and without chiral dopant spin-coated on a Gr–glass substrate before and after rotation. Without chiral dopant (a) 0° and (b) 90°, whereas, (c) 0° and (d) 90° with chiral dopant (these micrographs were recorded as 10× magnification).

the resonant mode in the aligned sample (inset in Fig. 4b and shows pump energy), and it is believed that, higher optical pump energy is needed to produce the necessary density of photonic states in the smaller helical domains in the Gr–Gr cell. The spectral emission profile of the Gr–Gr cell was found to be very similar to the case of an ITO–ITO cell without alignment (Fig. 4d). The only measureable difference being that the density of discrete peaks was found to be higher in the Gr–Gr cell, possibly corresponding to the relatively more disorder in the chiral helix texture that was observed in the optical micrographs (Fig. 1d).

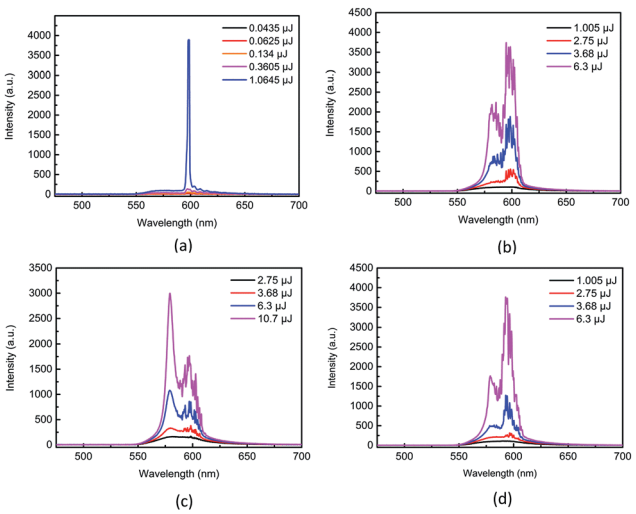

Fig. 4 Spectral profiles of the emission of the various laser cell configurations. (a) ITO–ITO, alignment layers, (b) Gr–Gr, (c) Gr–ITO, without alignment layer, the graphene side faces the pump laser in this case, and (d) ITO–ITO, without alignment layers.

In the case of hybrid electrode geometry (Gr–ITO) it can be clearly seen that the output is very different from that of the other architectures (the change in spectral output as a function of pump energy is illustrated in Fig. 4c). It was found that the emission around the band edge (590–600 nm) was suppressed, and instead there was gain seen around the eye emission maximum (580 nm). Furthermore, it was observed that the emission spectrum varies significantly depending on which substrate's surface is facing toward the light pump source. The spectrum (Fig. 4c) corresponds to the case where the graphene substrate is facing the optically pump source. When the pump light source is incident on the ITO side, the spectral contribution of lasing modes near the photonic band edge have comparatively enhanced emission lines (at the same pump energy, Fig. 5a, this is in stark contrast to the case where the pump light is incident on the graphene site first in which an enhanced peak of emitted light around the dye emission maximum is observed). The full-width at half maximum (FHWM) of the peak is observed to narrow with increasing pump energy (Fig. 4c), and at present we believe this to be either a manifestation of a precursor to non-resonant random lasing (due to enhanced scattering in the vicinity of the graphene layer), or super radiance/luminescence in the dye doped LC medium[23] The exact mechanism behind the narrowing and relative high intensity of the peak at 580 nm needs to be studied in further details, accompanied by an analysis on the photon statistics of the emitted light. The difference in emission characteristics, in the two cases is thought to be due to the scattering of pump light above the graphene surface, which might be contributing more towards an emission phenomena different from band-edge lasing.

This multi-domain nature of the dye-doped chiral nematic LC texture led to an array of sharp peaks in the emission spectrum in sandwich cells of Gr–Gr, Gr–ITO and ITO–ITO cells. In addition, owing to the variation in the LC domain structures in the Gr–ITO architecture, lasing characteristics exhibit significantly different output depending on substrate facing to

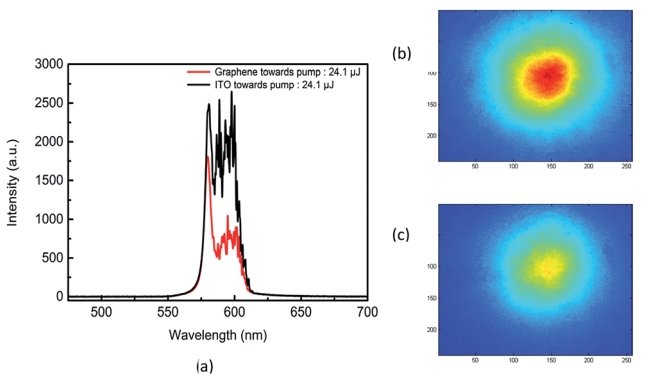

Fig. 5 Laser emission of Gr–ITO cell, (a) contrast between the emission spectrum of the Gr–ITO hybrid lasing cell, depending on which side the pump light is incident normally. The spatial profiles of emission spectra under optical pump energy of 14.35 μJ are illustrated in; (b) ITO side faces the optical pump source and (c) when Gr side faces the optical pump source.

the light pump source. The effect of an applied electric field on Gr–ITO cell emission characteristics was studied (Fig. 6; Fig. 6a illustrates the spectral response as electric fields are applied, and the accompanying LC textures are shown in Fig. 6b–d). The changes that have been observed in the LC textures are quite significant (ESI, Fig. S2†) though the intensity of fluorescence peak enhanced at applied field of 3 V μm^{-1}, no significant contrast has been found in the emission spectra under applied electric fields.

To further understand these emission features of the hybrid (Gr–ITO) laser device, a standard rubbed polyimide alignment layer was applied to ITO side in the test cell (Fig. 7a, illustrates a schematic of this device). Optical micrographs were recorded for two orientations under objective lens (graphene side faces-up Fig. 7c and faces-down, Fig. 7d). It can be seen that the LC texture is very different in both cases. When aligned ITO side is oriented towards the microscope objective the texture is more uniform (Grandjean texture) as compared to the graphene where the texture exhibited multi-domain disordered as a degenerated planar surface.

Optical transmission spectra (Fig. 7b) of the two sides are very similar, and there is a possibility that while the more disordered domain structure is more evident when the graphene side faces towards the light source, the overall average band edge characteristic dominates. However, as the optical micrographs suggest, such anisotropy in texture of the chiral nematic in a single device is interesting, and the devices were subsequently optically pumped to test lasing characteristics.

The lasing results for the Gr–ITO (with alignment layer) cell are depicted in Fig. 8. The emission spectrum for the case in which the graphene layer oriented towards the pump light source contains bright contributions from several wavelengths,

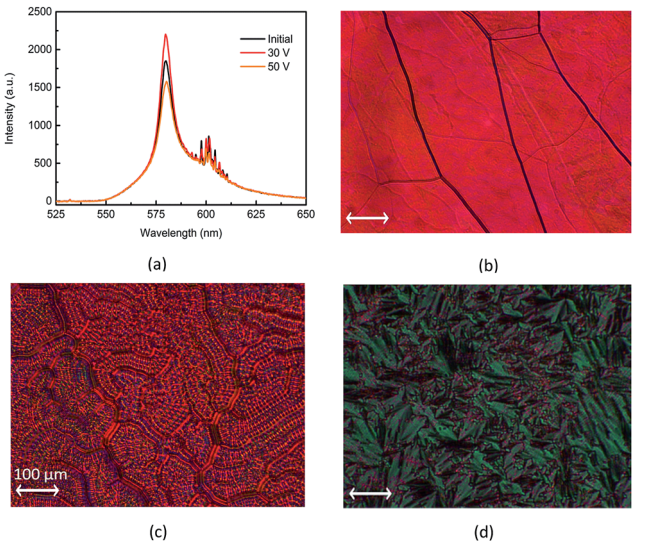

Fig. 6 The effect of applying electric fields to a Gr–ITO cell with an alignment layer, (a) illustrates the change in emission spectrum at different applied fields; (b) 0 V μm^{-1}, Grandjean texture, (c) 3 V μm^{-1} finger print texture, and (d) 7 V μm^{-1} appearance of focal conic, (the optical textures recorded under a 20× magnification).

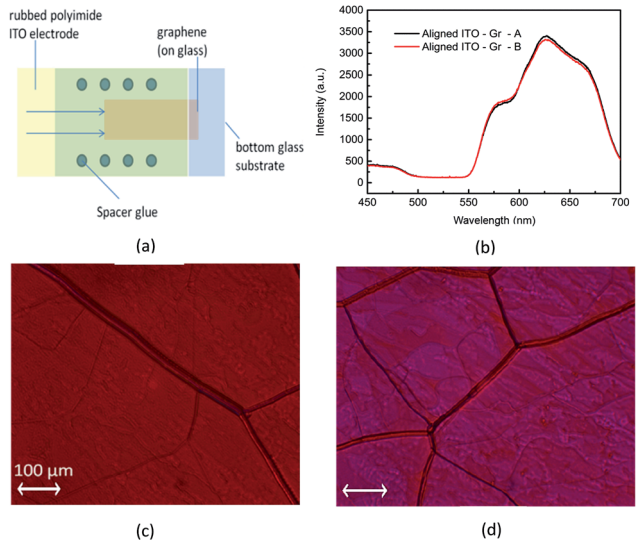

Fig. 7 Gr–ITO test cell, (a) schematic of a hybrid Gr–ITO lasing cell with alignment on the ITO electrode, (b) spectrum of the Gr–ITO (with alignment layer) cell under transmission microscopy, for two different orientations of the cell; (c) graphene side is facing up, and (d) the case with the ITO side is facing the microscope objective.

as opposed to the emission in the case where the ITO side is preferentially pumped (Fig. 8a).

However, the emission line-widths are much narrower and laser like in this device (for both orientations), especially in the case of ITO-side was facing light pump source. This

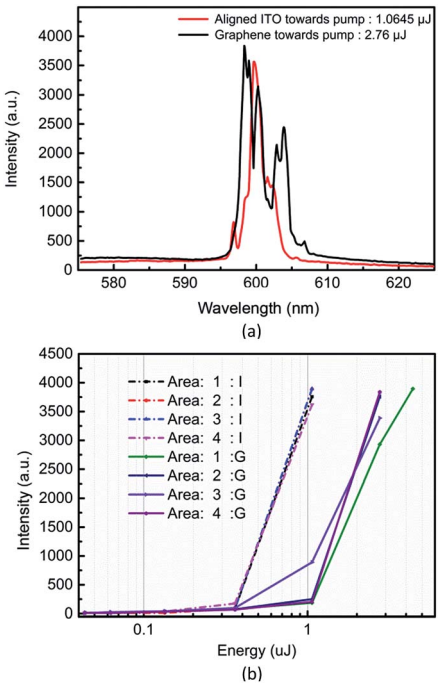

Fig. 8 Comparison of the laser emission spectra, (a) Gr–ITO cell (with alignment layer), (b) measured intensity as a function of optical pump energy across different regions in the lasing cell (I: ITO side towards pump light, G: graphene electrode towards pump light).

might seem intuitive at hindsight, as the alignment layer effectively reduces the amount of disorder in the system, but the noteworthy difference in spectral response of the devices (Fig. 5a and 8a) is nevertheless encouraging. This observation could prove important for possible future applications of these devices, in addition to future studies that study the emission characteristics and photon statistics of these laser devices.

An estimate of the laser pump threshold of the Gr–ITO (with alignment layer) device can be made from Fig. 8b. The pump energy was ramped up in discreet steps, and the output emission intensity is plotted across four different regions of the cell, for the two pumping orientations (graphene/ITO face). It is clear the pump threshold for the case where the ITO side is preferentially pumped is at least three times less ($\approx$350 nJ) than the case where the graphene substrate is facing toward the pump light source. It is possible that this stark difference is either due to the scattering of pump light above the graphene surface or due to a difference in the size and orientation of chiral domains close to the substrates.

4. Conclusions

The effect of using graphene alignment and electrodes layers in 1D photonic band edge N*LC devices has been studied, with a particular emphasis on lasing. It was found that hybrid electrode geometries (Gr–ITO) both with/without an alignment layer have shown some rather interesting results, with highly anisotropic output depending on the directionality of optical pumping of the lasers. We note that the actual LC texture upon interaction with the graphene sheets may make it very difficult to obtain single mode lasing from graphene band edge LC lasers. However, standing chiral helices with multidirectional orientations (tilted helical domains) on the surface of graphene demonstrates a unique prospect to fabricate devices with wide angle photonic structures (Fig. 2). This in turn could help to devise optical filters based on diffused chiral nematic phase, including notch filters, colour reflectors, and light shutters.[2,3,24–27] At present, these laser sources can be used to produce relatively multi-modal light source as a result of the tilted helical domains in the vicinity of the graphene layers. A possible direct application of these laser sources could be a quick characterization of the quality of grown graphene by sampling the graphene domain–domain variation emission characteristics under coherent pumping of the LC medium (needs in-depth study, emission characteristics with known domain lattices). Further examination of the polarization control/modulation and coherence properties of the hybrid graphene LC laser sources will be very important to determine future applications, such as the generation of speckle free holograms and consequently large area 3D displays.

Acknowledgements

This work was carried out under the GRAPHTED project which is funded by the Engineering and Physical Sciences Research Council UK (project ref. EP/K016636/1, Grant No. EP/H047565/1). A. A. K. would like to thank the Higher Education of Pakistan (HEC), P. R. K. acknowledges Lindemann Trust Fellowship. A. A. K. and P. R. K. acknowledge the Cambridge Commonwealth, European and International Trust and for the financial support.

References

1 T. J. White, R. L. Bricker, L. V. Natarajan, V. P. Tondiglia, C. Bailey, L. Green, Q. Li and T. J. Bunning, *Opt. Commun.*, 2010, **283**, 3434–3436.
2 S. M. Morris, M. M. Qasim, K. T. Cheng, F. Castles, D.-H. Ko, D. J. Gardiner, S. Nosheen, T. D. Wilkinson, H. J. Coles, C. Burgess and L. Hill, *Appl. Phys. Lett.*, 2013, **103**, 101105.
3 S. S. Choi, S. M. Morris, W. T. S. Huck and H. J. Coles, *Adv. Mater.*, 2009, **21**, 3915–3918.
4 C. Hilsum and D. G. McDonnell, Br. Patent 2085 585 B, 1984.
5 S. Ishihara, F. Yokotani, Y. Matsuo and K. Morimoto, *Polymer*, 1988, **29**, 2141–2145.
6 H. Coles and S. Morris, *Nat. Photonics*, 2010, **4**, 676–685.
7 Z. Zheng, B. Liu, L. Zhou, W. Wang, W. Hu and D. Shen, *J. Mater. Chem. C*, 2015, **3**, 2462–2470.
8 B. Liu, Z. Zheng, X. Chen and D. Shen, *Opt. Mater. Express*, 2013, **3**, 519–526.
9 V. I. Kopp, B. Fan, H. K. M. Vithana and a. Z. Genack, *Opt. Lett.*, 1998, **23**, 1707.
10 J. P. Dowling, M. Scalora, M. J. Bloemer and C. M. Bowden, *J. Appl. Phys.*, 1994, **75**, 1896.
11 P. Blake, P. D. Brimicombe, R. R. Nair, T. J. Booth, D. Jiang, F. Schedin, L. a. Ponomarenko, S. V. Morozov, H. F. Gleeson, E. W. Hill, A. K. Geim and K. S. Novoselov, *Nano Lett.*, 2008, **8**, 1704–1708.
12 D. W. Kim, Y. H. Kim, H. S. Jeong and H.-T. Jung, *Nat. Nanotechnol.*, 2012, **7**, 29–34.
13 J. Guo, C. M. Huard, Y. Yang, Y. J. Shin, K.-T. Lee and L. J. Guo, *Adv. Opt. Mater.*, 2014, **2**, 435–441.
14 Q. Zhang, Y. Di, C. M. Huard, L. J. Guo, J. Wei and J. Guo, *J. Mater. Chem. C*, 2015, **3**, 1528–1536.
15 Y. Iwakabe, M. Hara and K. Kondo, *Jpn. J. Appl. Phys.*, 1991, **30**, 2542.
16 J. Frommer, *Angew. Chem., Int. Ed. Engl.*, 1992, **31**, 1298–1328.
17 H. J. Gardiner, D. J. Hsiao, W. K. Morris, S. M. Hands, P. J. W. Wilkinson, T. D. Hutchings and I. M. & Coles, *24th Int. Liq. Cryst. Conf. (ILCC 2012)*, Mainz, Ger., 19–24 August 2014.
18 P. R. Kidambi, C. Ducati, B. Dlubak, D. Gardiner, R. S. Weatherup, M.-B. Martin, P. Seneor, H. Coles and S. Hofmann, *J. Phys. Chem. C*, 2012, **116**, 22492–22501.
19 P. R. Kidambi, B. C. Bayer, R. Blume, Z.-J. Wang, C. Baehtz, R. S. Weatherup, M.-G. Willinger, R. Schloegl and S. Hofmann, *Nano Lett.*, 2013, **13**, 4769–4778.
20 P. J. Collings and M. Hird, *Introduciton to Liquid Crystals*, Taylor & Francis, 1997.
21 D. I. Dierking, *Textures of Liquid Crystals*, Wiley, 2004.

22 I. Dierking, F. Gießelmann and P. Zugenmaier, *Liq. Cryst.*, 1994, **17**, 17–22.
23 F. C. Spano and S. Mukamel, *J. Chem. Phys.*, 1989, **91**, 683.
24 H. J. Masterson, G. D. Sharp and K. M. Johnson, *Opt. Lett.*, 1989, **14**, 1249.
25 G. D. Sharp, K. M. Johnson and D. Doroski, *Opt. Lett.*, 1990, **15**, 523.
26 M. Mitov, E. Nouvet and N. Dessaud, *Eur. Phys. J. E: Soft Matter Biol. Phys.*, 2004, **15**, 413–419.
27 D.-K. Yang, L.-C. Chien and J. W. Doane, *Appl. Phys. Lett.*, 1992, **60**, 3102.